Chapter 5
Creep with Low Stress Exponents

Abstract Primary creep models predict that at low stresses a stress exponent of 1 can be obtained for dislocation creep. Also experimentally this has been observed for an austenitic stainless steel. The time dependence of the primary creep verifies that it is dislocation creep. An other example is for Al at very high temperatures (Harper-Dorn creep), where at sufficiently low stresses, the stress exponent approaches 1. For both materials higher stresses give larger stress exponents as expected for dislocation creep. Obviously, diffusion and dislocation creep can be competing processes. The validity of creep models at low stresses and high temperatures as well as at high stresses and low temperatures demonstrates their wide range of usage. Since this in reality represents an extensive extrapolation, it can be consider as a direct verification of the basic creep models. In cases for Cu and stainless steels, the predicted creep rate by diffusion creep (Coble) exceeds the observed creep rate as well as the predicted one by dislocation creep by an order of magnitude. The likely explanation is that constrained boundary creep is taken place, i.e. the grain boundary creep rate cannot be essentially faster than that of the bulk.

5.1 General

Creep at low stresses has generated great interest amongst scientists for a long time. Expressions for diffusional creep that do not involve dislocations were developed at an early stage. First an expression based on bulk diffusion was formulated [1]. This is now referred to as Nabarro-Herring creep. The creep takes place by diffusion from grain boundaries with low stresses to boundaries located perpendicular to the loading direction. An alternative expression was given by Coble [2] where the diffusion is assumed to take place in the grain boundaries instead of in the bulk. The difference in diffusion mechanism means that Nabarro-Herring creep is proportional to the bulk diffusion coefficient and Coble creep to the grain boundary diffusion coefficient. The grain size dependence is also different. With bulk diffusion the creep rate is inversely proportional to the square of the grain size. With grain boundary diffusion

R. Sandström, *Basic Modeling and Theory of Creep of Metallic Materials*, Springer Series in Materials Science 339,
https://doi.org/10.1007/978-3-031-49507-6_5

the proportionality is instead to the inverse cube of the grain size. Models for diffusion creep is summarized in Sect. 5.2.

The derivations for diffusional creep gave the first basic equations for the creep rate. The expressions do not involve any arbitrary or adjustable parameters and the equations are fully predictable. For both types of diffusional creep, the rate is proportional to the stress, which means that the stress exponent is 1. Thus diffusional creep has a number of characteristic features: well defined dependence of the grain size, stress and temperature (through the diffusion coefficient). For a long time it was also assumed that a stress exponent of 1 should always be associated with diffusional creep. Authors have suggested observations of Herring-Nabarro or Coble creep in many metals: Cd, Co, Cu, Fe, Mg and Zr. Kassner has given an excellent review of diffusional creep [3] and details about the observations and references can be found there.

Observations of diffusional creep have often been controversial. One reason is that observed creep rates have not been in agreement with predicted ones in a number of studies [4]. In for examples the excellent studies on βCo and αFe [5, 6], the observed creep rate was about two orders of magnitude higher than the predicted ones. The identification of diffusional creep is not necessarily based only on the observed creep rates. There are also metallographic techniques to distinguish between dislocation and diffusional creep. Langdon proposed that if scratches are made parallel to the loading direction, the markings would be still continuous across the grain boundaries after the test for dislocation creep but not for diffusional creep [7]. This requires that no grain boundary sliding occurs along the considered boundaries. Another proposal is that diffusional creep gives denuded zones in particle hardened alloys or grooves around grain boundaries [8, 9]. For example, McKnee et al. have used these techniques to support observations of diffusional creep [10, 11]. The role of denuded zones has been questioned in the literature [12]. Ample evidence is now available that demonstrates that denuded zones can be formed also during dislocation creep. Wadsworth et al. suggest that denuded zones are created at grain boundaries that are sliding and migrating simultaneously [13].

When recording creep rates during diffusional creep, it is assumed that stationary conditions have been reached. In creep testing at higher stress, the deformation can be allowed to continue until rupture takes place. Then it is straightforward to determine when the stationary stage has been reached. During dislocation creep, a distinct primary stage is expected. If such a stage is observed it is an indication that the operating mechanism is not diffusional creep. However, as will be discussed in this chapter, it is possible that diffusional creep can also show primary creep. It is evident that in many cases it is quite difficult to decide when stationary conditions have been achieved. If the creep rate is assessed during the primary stage, the measured creep rate would typically be much higher than in the secondary stage. In addition, the stress exponent can be low also for dislocation creep often approaching a value of 1. This makes it easy to mistake it for diffusional creep. Modeling can be quite helpful in understanding non-stationary conditions. In this chapter, modeling is presented that can assess and interpret creep rates that are measured in the primary stage, Sect. 5.5.

Harper and Dorn tested aluminum very close to the melting point at very low stresses looking for diffusional creep [14]. Their results gave a stress exponent of 1 but the creep rate was two orders of magnitude higher than the diffusional creep models predicted. They draw the conclusion that the mechanism was dislocation creep with a stress exponent of 1. This phenomenon is referred to as Harper-Dorn creep. It has created large interest. The work in the area is summarized in a paper by Kassner et al. [15]. Some authors were able to reproduce the results of Harper and Dorn [16, 17], others were not [18]. It was early on suspected that in many cases stationary conditions had not been reached. This has been confirmed in a paper by Kumar et al. [19] where the testing was carried to somewhat larger strains. The stress exponent now took the value of 3. They also found that Harper and Dorn had introduced a threshold stress, which Kumar et al. could not find any justification for. If the threshold stress is removed also the Harper and Dorn data are consistent with a stress exponent of 3 so the whole effect disappears. In Sect. 5.7, creep at very low stresses in aluminum is modeled. It is shown that deviations from a stress exponent of 3 can be explained by taking non-stationary effects into account. Thus, creep at very low stresses at high temperature can be fully accounted for with ordinary dislocation creep models and there is no need to refer to Harper-Dorn creep as a special effect.

Tests at very low stresses for the austenitic stainless steel 316H and the martensitic steel P91 have given a stress exponent of 1 [20]. Since distinct primary creep is observed and stress change experiments gave a stress exponent of 4.5 [21], it is concluded that the operation mechanism is dislocation creep. The tests for 316H are analyzed with a primary creep model in Sect. 5.6. The non-stationary model can quantitatively explain the behavior at low stresses (and at higher stresses). This clearly demonstrates that dislocation creep can be of importance also at very low stresses.

Creep tests that have claimed to demonstrate diffusional creep for Cu [9, 22], have been analyzed in Sect. 5.8. It is shown that the part of the experimental data that has been investigated is possible to reproduce with non-stationary dislocation creep. There are pros and cons whether these observations represent diffusional or dislocation creep. Further details are given in Sect. 5.8.

Results for previously unpublished results on creep in Cu between and 1 and 2 MPa at 600° C are presented. The tests are unusual for low stress experiments since the testing times exceed 12000 h. The results clearly represent dislocation creep, since the stress exponent is 3 and distinct primary creep is observed. Furthermore the results are in good agreement with the basic model for stationary creep, so any non-stationary model is not needed. The surprising feature is that the Coble creep model suggests a creep rate that exceeds the observations by an order of magnitude or more. Although mechanisms have been proposed in the literature that can reduce the Coble creep rate, it is difficult to identify such a mechanism in this case that can explain the effect. This is further discussed in Sect. 5.8.1. Also for the investigated case for 316H, Coble creep overestimates the observed creep rates at low stresses (by about one order of magnitude).

The classical diffusional models are briefly derived and summarized in Sect. 5.2. To explain the effect of alloying elements on the diffusional creep rate, several authors

assume that mobile grain boundary dislocations are a prerequisite for diffusional creep. For this reason a recovery creep model for grain boundary dislocations is formulated in Sect. 5.3. It is demonstrated that the grain boundary dislocations can give rise to quite a high creep rate, a phenomenon that does not seem to be covered in the literature. Some results suggest that creep along the grain boundaries must be accompanied with simultaneous deformation in the grains. This is covered in Sect. 5.4. It is referred to as constrained grain boundary creep. In Sect. 5.5, the primary creep model that is used to describe non-stationary dislocation creep at low stresses is summarized. Applications of the primary creep model at low stresses for an austenitic stainless steel are given in Sect. 5.6, for aluminum in Sect. 5.7, and for copper in Sect. 5.8.

5.2 Model for Diffusional Creep

Detailed models for diffusional creep were already presented in the original papers for Nabarro-Herring and Coble creep [1, 2]. Here, only a simplified derivation will be given. During Nabarro-Herring creep in tension, matter is transported to grain boundaries oriented perpendicular to the loading direction from grain boundaries parallel to the loading direction. This is possible by migration of vacancies in the opposite direction. It is assumed that the sources and sinks of the vacancies are at the grain boundaries. This is opposite to dislocation creep where the sinks and sources are primarily at the dislocations. The difference in vacancy concentration Δc_v between the boundaries that are exposed to a stress σ and the others is

$$\Delta c_\mathrm{v} = \exp\left(-\frac{Q_\mathrm{F}}{k_\mathrm{B}T}\right)\left(\exp\left(\frac{\sigma v_\mathrm{atom}}{k_\mathrm{B}T}\right) - 1\right) \tag{5.1}$$

Q_F is the vacancy formation energy and v_atom the atomic volume. The first factor in Eq. (5.1) is the thermal equilibrium concentration of vacancies. The second factor describes the increase in vacancy concentration due to the presence of the stress. Since only low stresses are considered, Eq. (5.1) can be rewritten as

$$\Delta c_\mathrm{v} = c_\mathrm{v0}\frac{\sigma v_\mathrm{atom}}{k_\mathrm{B}T} \tag{5.2}$$

A notation c_v0 has been introduced for the equilibrium vacancy concentration. The flow of vacancies J can be expressed as

$$J = -\frac{D_\mathrm{v}}{v_\mathrm{atom}}\frac{\Delta c_\mathrm{v}}{d_\mathrm{eff}} = -D_\mathrm{v}\frac{c_\mathrm{v0}}{d_\mathrm{eff}}\frac{\sigma}{k_\mathrm{B}T} \tag{5.3}$$

D_v is the vacancy diffusion coefficient and d_eff the effective diffusion distance. For a simple grain structure, d_eff can be estimated. Let us assume that we have coordinates

x and y on perpendicular grain boundaries in a quadratic grain

$$d_{\text{eff}} = \frac{1}{d_{\text{grain}}^2} \int_0^{d_{\text{grain}}/2} \int_0^{d_{\text{grain}}/2} \sqrt{x^2 + y^2} dx dy = 0.1 d_{\text{grain}} = \frac{d_{\text{grain}}}{A_{\text{NH}}} \tag{5.4}$$

The constant A_{NH} has been introduced to mark that its value depends on the geometry of the grains. The vacancy flux gives rise to a change in the grain size along the loading direction

$$\frac{d d_{\text{grain}}}{dt} = -J v_{\text{atom}} \tag{5.5}$$

This corresponds to a creep rate $\dot{\varepsilon}_{\text{NH}}$ of

$$\dot{\varepsilon}_{\text{NH}} = \frac{1}{d_{\text{grain}}} \frac{d d_{\text{grain}}}{dt} = \frac{J v_{\text{atom}}}{d_{\text{grain}}} = A_{\text{NH}} D_{\text{v}} \frac{c_{\text{v0}}}{d_{\text{grain}}^2} \frac{\sigma v_{\text{atom}}}{k_{\text{B}} T} \tag{5.6}$$

where Eq. (5.3) has been inserted for J. The expression for d_{eff} in Eq. (5.4) has also been used where $A_{\text{NH}} = 10$. The vacancy diffusion coefficient D_{v} is related to the self-diffusion coefficient D_{latt}

$$D_{\text{latt}} = D_{\text{v}} c_{\text{v0}} \tag{5.7}$$

If this expression is applied the final expression for the Nabarro-Herring creep rate is obtained.

$$\dot{\varepsilon}_{\text{NH}} = A_{\text{NH}} \frac{D_{\text{latt}}}{d_{\text{grain}}^2} \frac{\sigma v_{\text{atom}}}{k_{\text{B}} T} \tag{5.8}$$

The result in Eq. (5.8) is identical to the original expression derived by Herring for quadratic grains [1]. However, it is more common to use the expression for spherical grains and then $A_{\text{NH}} = 14$ instead of 10 [1, 23]. Greenwood has presented expressions for Nabarro-Herring creep for more general grain structures [24].

It is possible to extend the equation to Coble creep by introducing an effective diffusion coefficient D_{eff} that takes both lattice diffusion and grain boundary diffusion into account

$$D_{\text{eff}} = D_{\text{latt}} \left(1 + \frac{\pi \delta_{\text{GB}}}{d_{\text{grain}}} \frac{D_{\text{GB}}}{D_{\text{latt}}} \right) = D_{\text{latt}} \left(1 + \frac{\pi}{d_{\text{grain}}} \frac{\delta D_{\text{GB}}}{D_{\text{latt}}} \right) \tag{5.9}$$

where δ_{GB} is the grain boundary width. In this book the grain boundary diffusion coefficient is represented by δD_{GB} that includes the grain boundary width and has the unit m^3/s. This is the quantity that is most often measured. But Eq. (5.9) is also expressed in terms of the grain boundary diffusion coefficient D_{GB} that does not

include δ_{GB} and has the unit m^2/s. The factor π in front of δD_{GB} can take different values in different sources but π is the most common choice. If D_{latt} is replaced by D_{eff} in Eq. (5.8), Coble creep is covered by the second term in the brackets

$$\dot{\varepsilon}_{diffcreep} = A_{NH} \frac{\sigma v_{atom}}{k_B T d_{grain}^2} D_{latt} \left(1 + \frac{\pi}{d_{grain}} \frac{\delta D_{GB}}{D_{latt}}\right) \tag{5.10}$$

5.3 Grain Boundary Creep

As will be seen in Sects. 5.6 and 5.8, the classical model for Coble creep can overestimate the observed creep rates by at least an order of magnitude. This means that diffusional creep must be blocked by one or more processes. Such processes have been proposed. A survey of earlier work is provided by Arzt et al. [25]. The diffusion process in the grain boundary can be affected. However, it is difficult to see how such processes can provide mechanisms that are sufficient large to explain the mentioned observations. In a number of papers including [25], it assumed that dislocation activities are needed to make grain boundaries involved in diffusional creep and provide the necessary sources and sinks of vacancies. This gives a way to explain the large blocking effects. Another mechanism that does not seem to have been raised in the literature, is that the dislocations in the grain boundaries can give a direct contribution to the creep rate without involving diffusional creep. In this section, a model is presented for this contribution. In the derivation, due to the lack of access, specific properties for grain boundary dislocations will not be used. Instead, parameters for bulk dislocations will be applied.

The first step is to formulate a model for development of the dislocation density during creep in the grain boundaries equivalent to Eq. (2.17). In the same way as for deformation in the bulk, the starting point is the Orowan Eq. (2.6). It has a different form for GB dislocations [26]

$$\dot{\varepsilon} = \frac{b_n \rho v_{disl}}{m_T d_{grain}} \tag{5.11}$$

where b_n is the component of the Burgers vector perpendicular to the GB, ρ the dislocation density and v_{disl} the velocity of the dislocations. Equation (5.11) is integrated and derivated with respect to the strain to give

$$\frac{d\rho}{d\varepsilon} = \frac{m_T d_{grain}}{b_n L_s} \tag{5.12}$$

L_s is the spurt distance, cf. Eq. (2.5) and it is assumed that it can be expressed in the subgrain diameter d_{sub}. In the same way as for bulk deformation

$$L_s = n_{sub} d_{sub} \tag{5.13}$$

where the constant n_{sub} is close to 3 [27, 28]. The subgrain size can be related to the dislocation stress

$$d_{sub} = \frac{K_{sub} G b}{\sigma_{disl}} \tag{5.14}$$

K_{sub} is a constant typically in the range 10–20. The expression for the Taylor Eq. (2.20) has to be modified [25]

$$\sigma_{disl} = \alpha m_T G b \rho = \sigma - \sigma_i \tag{5.15}$$

The dislocation stress σ_{disl} is now linear in the density. σ_i is the back stress from solid solution and particle hardening. By combining Eqs. (5.11)–(5.15) it is found that the change in the dislocation density contributing to the work hardening is given by

$$\frac{d\rho}{d\varepsilon} = \frac{m_T d_{grain}}{b c_L} \rho \qquad \text{(work hardening)} \tag{5.16}$$

where

$$c_L = \frac{n_{sub} K_{sub}}{m_T \alpha} \tag{5.17}$$

In comparison to the bulk Eq. (2.9), the difference is that the work hardening contribution is linear in the dislocation density. Since the dislocation stress σ_{disl} is linear in the dislocation density, the strain dependence of σ_{disl} is also linear.

$$\frac{d\sigma_{disl}}{d\varepsilon} = \frac{m_T d_{grain}}{c_L b_n} \sigma_{disl} \qquad \text{(work hardening)} \tag{5.18}$$

For the elastic properties and the Burgers vector for example in Eq. (5.15), grain boundary values should be applied. However, for metals the values of the elastic properties are of the order of 93% of the bulk values [29]. Considering the uncertainties involved in modeling grain boundary properties, these replacements have not been made.

For the static recovery, the starting point is Eq. (2.16).

$$\frac{dR}{dt} = \frac{M_B \tau_L}{R} \tag{5.19}$$

where R is the spacing between dislocations and τ_L the dislocation line tension. The boundary climb mobility is given by

$$M_B = \frac{bD_{GB}}{k_B T} \tag{5.20}$$

Notice the difference between the two grain boundary diffusion coefficients

$$\delta D_{GB} = \delta_{GB} D_{GB} \tag{5.21}$$

δD_{GB} and D_{GB} have the units m^3/s and m^2/s, respectively. δ_{GB} is the grain boundary width that is usually taken as 5×10^{-10} m. The dislocation spacing R in the boundary is

$$R = 1/\rho \tag{5.22}$$

Inserting Eq. (5.22) into (5.19) gives

$$\frac{d\rho}{dt} = -\tau_L M_B \rho^3 \qquad \text{(static recovery)} \tag{5.23}$$

There are two differences between Eq. (5.23) and the bulk version, Eq. (2.13). First, the factor of 2 is missing and the dislocation density appears to the third order. By summing the contributions from Eqs. (5.16) and (5.23), an expression for the strain dependence of the dislocation density is obtained

$$\frac{d\rho}{d\varepsilon} = \frac{m_T d_{grain}}{bc_L}\rho - \tau_L M_B \rho^3 / \dot{\varepsilon}_B \tag{5.24}$$

The time derivative in Eq. (5.23) has been changed to a strain derivative by dividing by the strain rate. $\dot{\varepsilon}_B$ is the local creep rate in the grain boundary. During stationary condition the strain derivative of the dislocation density vanishes and the creep rate can be found directly. The overall grain boundary creep rate $\dot{\varepsilon}_{GB}$ is given by

$$\dot{\varepsilon}_{GB} = \frac{\delta_{GB}}{d_{grain}}\dot{\varepsilon}_B = \frac{\delta_{GB} b c_L \tau_L M_B \rho^2}{d_{grain}^2 m_T} \tag{5.25}$$

With the modified Taylor, Eqs. (5.15) and (5.25) can be expressed in terms of stress

$$\dot{\varepsilon}_{GB} = \frac{\delta_{GB} b c_L \tau_L M_B (\sigma - \sigma_i)^2}{d_{grain}^2 m_T (\alpha m_T G b)^2} \tag{5.26}$$

The grain boundary creep rate is inversely proportional to the square of the grain size and has a stress exponent of about 2 at low stresses. At higher stresses the role of pipe diffusion, strain induced vacancies, etc. should be taken into account in the same way as for creep in the bulk. Equation (5.26) has the same temperature, stress

and grain size dependence as the creep rate during superplastic deformation due to GBS, Eq. (9.20), but the equations are not identical.

Equation (5.26) can give quite a high strain rate. The grain boundary diffusion coefficient is much larger than the bulk diffusion coefficient and that is only compensated to some extent by the ratio δ_{GB}/d_{grain}. It is important to take into account the role of cross-slip. If the grain boundaries are fully straight, cross-slip has to take place at the triple points. However, the boundaries are often curved, and then cross-slip is continuous. With cross-slip an extra activation energy has to be introduced, Eq. (2.47)

$$g_{\text{cross-slip}} = \exp\left(-\frac{E_{cs}}{R_G T}\right) \tag{5.27}$$

Equation (5.26) is multiplied by Eq. (5.27). The problem is that the value of the activation energy for cross-slip is uncertain. As summarized in Sect. 2.6.3, ab initio values for the activation energy vary from 50 to 270 kJ/mol. The values for alloys appear to be larger than for pure metals. The role of cross-slip remains an open issue.

5.4 Constrained Grain Boundary Creep

Creep in the grain boundaries without plastic deformation in the neighboring grain interiors is not possible. Perhaps, the most obvious effect is for superplasticity. In this case the main deformation takes place by GB sliding. However, extensive deformation cannot occur in a material without the grain interiors being affected. In other words, creep in the grain boundaries must always be accompanied by creep in the whole grains as well. This phenomenon will be referred to as *constrained grain boundary creep*. The term is taken from growth of creep cavities that inside a material growth cannot be faster than the creep deformation, see Sect. 10.5.2.

Grain boundary creep according to Eq. (5.26) can give quite a high creep rate, in many cases higher than bulk dislocation creep, but such a phenomenon has not been reported in the literature. It is assumed that the grain boundary creep rate $\dot{\varepsilon}_{GB}$ cannot exceed the creep rate in the bulk $\dot{\varepsilon}_{bulk}$ significantly. The bulk creep mechanism is practically always dislocation creep but could in principle also be Nabarro-Herring creep. If the grain boundary creep rate $\dot{\varepsilon}_{GB}$ is estimated to be higher than the bulk creep rate, the creep rates must be matched approximately

$$\dot{\varepsilon}_{GB}(\sigma_{red}) \approx \dot{\varepsilon}_{bulk}(\sigma) \tag{5.28}$$

Thus, the stress controlling the grain boundary creep rate must be reduced to ensure that the creep rates match.

In Sects. 5.6 and 5.8.1 it is shown that the Coble creep model rates can exceed the observations by more than an order of magnitude. Several mechanisms have been proposed that could retard diffusional creep. These are in general based on the

assumption that the creep rate is controlled by GB dislocations [25]. For Nabarro-Herring creep, they can account for that GBs are not perfect sources and sinks for vacancies. For Coble creep the GB dislocations assure that atoms and vacancies can leave the GBs to avoid that they are getting saturated. Many mechanisms are available that can reduce the mobility of GB dislocations. Further details are given in the mentioned sections.

If the estimated Coble creep rate is still higher than the bulk creep rate, constrained GB creep is active. This means that Eq. (5.28) must be satisfied for Coble creep as well

$$\dot{\varepsilon}_{\text{Coble}}(\sigma_{\text{red}}) \approx \dot{\varepsilon}_{\text{bulk}}(\sigma) \tag{5.29}$$

Thus, if the Coble creep rate is nominally higher than the bulk creep rate, matching of the two creep rates must take place and the stress driving Coble creep is reduced. Exceptions to this principle can be found for hypothetical grain structures. A grain structure consisting of identical rectangular prisms where there is a homogeneous padding of atoms on the planes perpendicular to the loading directions is an example where bulk deformation may not take place. Such cases have of course no practical relevance.

When the bulk creep rate is controlled by dislocation creep, it shows a higher creep rate in the primary stage and this allows Coble creep to have a higher creep rate initially as well. This means that Coble creep can have a primary stage. The main conclusion of this section is that any creep deformation mechanism that is entirely concentrated to the GBs cannot be significantly faster than the bulk creep rate.

5.5 Primary Creep at Low Stresses

One major concern when making creep tests at low stresses is whether stationary conditions have been reached. Most creep models refer to the stationary creep rate when identifying creep mechanisms. If the creep test has not been carried out long enough the wrong conclusions can be drawn. At low stresses, the interesting question is often if diffusional or dislocation creep is observed. The stress exponent for diffusional creep is always assumed to be 1 according to the models for Nabarro-Herring and Coble creep. A possible exception exists for nanocrystalline alloys. It has been proposed that Coble creep can appear also at higher stresses and with a stress exponent larger than unity [30]. This possibility will not be considered here. If stationary creep has been reached, the stress exponent is 3 or more for dislocation creep. The known exception is superplasticity where the stress exponent can be 2. This is discussed in Sect. 9.4. Then it is straightforward to distinguish between diffusional and dislocation creep. However, if dislocation creep is in the primary stage, the stress exponent can be lower and the identification can be difficult.

In recent years basic models for primary creep have been developed. They are described in Chap. 4. With the help of these models a better understanding of the

creep behavior during non-stationary conditions can be established. Low stresses are often associated with low strains. The appropriate model is given in Eqs. (4.13) and (4.14). The model is called *stress adaptation*. In the same way as for the other models for primary creep in Chap. 4, the starting point is the creep rate in the stationary stage and the rate in the primary stage is related to that in the stationary stage. The only change is that an effective stress is introduced that is higher than the stationary stress, which can represent the higher creep rate in the primary stage. In the stress adaption model the effective stress is given by [31]

$$\sigma_{\text{primSA}} = \sigma_{\text{y}}(T, \dot{\varepsilon}) + \frac{\sigma - \sigma_{\text{y}}(T, \dot{\varepsilon})}{1 - e^{-\Omega\varepsilon/2}} \tag{5.30}$$

The quantity σ_{y} is the yield strength that depends on temperature and the strain rate $\dot{\varepsilon}$, Ω is related to the dynamic recovery constant, and σ the applied stress in the creep test. One requirement on the effective stress is that it tends to the applied stress at large strains. This is obviously the case in Eq. (5.30). The second part of the model is the rate for stationary creep, Eq. (4.3)

$$\dot{\varepsilon} = h(\sigma - \sigma_{\text{i}}) \quad \text{with} \quad h(\sigma) = \frac{2\tau_{\text{L}} b c_{\text{L}} M(T, \sigma)}{m_{\text{T}}} \frac{\sigma^3}{(\alpha m_{\text{T}} G b)^3} \tag{5.31}$$

where m_{T} is the Taylor factor, b burgers vector, G the shear modulus, c_{L} and α dimensionless constants, τ_{L} the dislocation line tension and M the dislocation climb mobility. σ_{i} is an internal stress that includes contributions from solid solution hardening and particle hardening. If the effective stress in Eq. (5.30) is inserted into (5.31), an expression for the creep rate is obtained that is valid for primary and stationary creep

$$\frac{d\varepsilon}{dt} = h\left(\sigma_{\text{y}}(T, \dot{\varepsilon}) + \frac{\sigma - \sigma_{\text{y}}(T, \dot{\varepsilon})}{1 - e^{-\Omega\varepsilon/2}} - \sigma_{\text{i}}, T\right) \tag{5.32}$$

Equation (5.32) is complicated but not impossible to integrate, since σ_{y} depends on the strain rate. This means that the equation has to be solved by iteration in each integration step. In addition, the primary stress in Eq. (5.30) is singular at small strains. However, it was demonstrated in Sect. 4.4.2 that these difficulties can be avoided. Equation (5.32) can be reformulated and the most suitable form is given in Eq. (4.25)

$$\dot{\varepsilon} = h\left(\frac{\sigma(\sigma_{\text{y}}(T) + K(T))}{\sigma_{\text{y}}(T) + K(T)(1 - \text{e}^{-\Omega\varepsilon/2})} - \sigma_{\text{i}}, T\right) \tag{5.33}$$

where $K(T)$ is given by

$$K(T) = \frac{\alpha G m_{\text{T}}^2}{\omega c_{\text{L}}} = \sigma_{\text{sat}}(T) - \sigma_{\text{y}}(T) \tag{5.34}$$

The saturation stress (maximum stress) σ_{sat} during plastic deformation at constant strain rate is the sum of $\sigma_y(T)$ and $K(T)$. In Eq. (5.33), the strain rate dependence of $\sigma_y(T)$ and $K(T)$ has been eliminated. These quantities are assumed to be influenced by the strain rate in the same way. This means that their values can in principle be selected at any strain rate.

Up to the creep range, the temperature dependence of σ_y and K are at least approximately known. The temperature dependence of the yield strength is proportional to that of the shear modulus, Eq. (3.15). The temperature dependence of the dynamic recovery constant ω is inversely proportional to that of the square of the shear modulus. However, in the creep range the increase in ω can be much faster with temperature. This is illustrated in Fig. 3.13. The role of Ω is that it describes how large the strain must be before the stationary or semi-stationary stage is reached. If the primary data are close to stationary conditions, the value of Ω can be assumed to be equal that of ω. However, if this is not the case, Ω is given by another expression, Eq. (4.33)

$$\Omega \approx \frac{3}{\varepsilon_{stat}} = \frac{3\alpha G m_T^2}{2c_L(\sigma - \sigma_i)} \tag{5.35}$$

To understand the behavior of Eq. (5.33) a simplified version is presented in Sect. 4.4.2. The strain dependence follows the ϕ model with a ϕ value of $n_N/(n_N + 1)$. Some requirements must be fulfilled. In particular, the following criterion must be satisfied, Eq. (4.30)

$$\frac{\sigma_y}{K} < \frac{\Omega\varepsilon}{2} \tag{5.36}$$

5.6 Creep at Low Stresses in an Austenitic Stainless Steel

In this section, creep of the austenitic stainless 17Cr12Ni2Mo steel 316H will be analyzed at low stresses. The creep data is taken from a paper of Kloc et al. [20] and the analysis from [32]. Very low stresses could be reached with the help of a helicoid spring specimen technique. Some of the experimental results are shown in Fig. 5.1.

The creep strain rate versus stress is given in Fig. 5.1. Two distinct regions of stress dependence are evident. At low stresses the stress exponent is about 1. At higher stresses, the stress exponent is 7, i.e. in the range for power-law creep. With a stress exponent of 1, it was initially thought that diffusional creep was observed. However, the presence of primary creep, see Fig. 5.1b suggests that dislocation creep is the controlling mechanism also at low stresses. In [20] similar creep tests were also performed for the 9Cr1Mo (P91) steel at 650 °C demonstrating a stress exponent of 1 at low stresses and a stress exponent of 12 at high stresses. For P91 stress change experiments were performed resulting in a stress exponent of 4.5 verifying dislocation

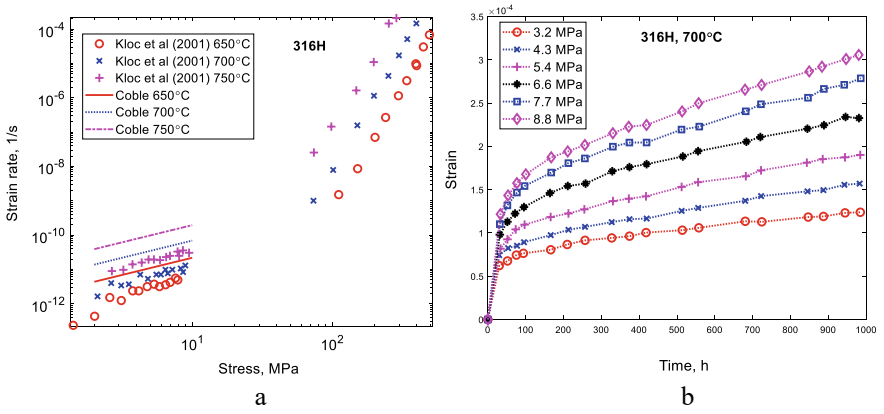

Fig. 5.1 Creep data for the austenitic stainless 17Cr12Ni2Mo steel 316H; **a** strain rate versus stress at 650–750 °C (exp.) and Coble creep model; **b** creep strain versus time at 700 °C for six stresses (creep data from [20]). Redrawn from [32] with permission of Elsevier

creep [21]. It can be expected that similar results would have been obtained for 316H if stress change experiments had been carried out. The creep rates at low stresses were assessed after testing for 1000 h. The natural interpretation of these results is that 1000 h is not long enough to reach stationary conditions. The consequences of this will be analyzed below.

In Fig. 5.1, predictions with the classical Coble model, Eq. (5.10) are included. It can be seen that the Coble model over predicts the observations by about one order of magnitude. The grain boundary diffusion coefficient from Smith and Gibbs has been used [33]. Their measurements are in the same temperature range as the creep data. However, the results are sensitive to the choice of diffusion coefficient. If the value from Mizouchi et al. [34] is chosen instead, the Coble predictions would be three orders of magnitude above the observations. Nabarro-Herring creep is not marked in the Figure but it gives values about an order of magnitude below the experimental data. Several papers in the literature address the problem that the diffusional models can overestimate the creep rate. A summary of early work is given by [25]. In these papers it is in general assumed that the required vacancies during diffusional creep are generated by the motion of GB dislocations. In some papers, a related concept of disconnections is considered, but the equations and effects are not very different from those of GB dislocations [35] and no distinctions between these concepts will be made here.

The main idea in these papers is that for Nabarro-Herring creep, GB dislocations are needed to emit and absorb vacancies at the GBs, since the GBs cannot be assumed to be perfect sources and sinks for vacancies. If the motion of GB dislocations is slowed down, it will impair the access of vacancies and reduce the creep rate. For Coble creep, the GB must be able to emit and absorb atoms and vacancies to avoid being over-saturated. This role of GB dislocations makes it easy to explain

deviations from the classical models. Mo in 316H gives a large solid solution hardening effect that reduces the creep rate dramatically. The influence of Mo has not yet been predicted but it can be assumed that it is of the same order as that of W, which raises the activation energy by about 50 kJ/mol [36]. This might seem like a high value but if the creep activation energy is assessed from the NIMS data [37], a value of 487 kJ/mol is obtained which should be compared with the activation energy for self-diffusion of 293 kJ/mol for 316H. Thus, the activation energy for creep is almost 200 kJ/mol higher than that for self-diffusion. The largest contribution to this increase comes from Mo. Therefore, a value of 50 kJ/mol for Mo that gives an Arrhenius factor of 0.002 at 700 °C is likely to underestimate its effect. The solid solution hardening effect can be assumed to be about the same for GB and bulk dislocations. As a consequence solid solution hardening alone can explain the deviation from the classical expression for Coble creep.

Particles can also influence the motion of dislocations in the grain boundaries. Arzt et al. suggest that a threshold stress σ_{th} is formed of about [25]

$$\sigma_{th} \approx 0.1\sigma_O \tag{5.37}$$

where σ_O is Orowan stress, Eq. (7.3). If typical values for $M_{23}C_6$ carbides are assumed with a volume fraction of 0.005 and particle radius of 0.1 mm, a σth value of 1.6 MPa is obtained. Such a threshold stress would certainly influence the prediction, but would not have a dramatic effect on the results. However, for other austenitic stainless steels the Orowan stress could be much higher. This could block diffusional creep completely if Eq. (5.37) describes the situation correctly and climb across particles is ignored. There are further constraints on grain boundary dislocations. But they are primarily of interest for pure metals. These constraints will be discussed in connection with creep of copper at low stresses in Sect. 5.8.

If the Coble creep rate taking these effects into account would still be higher than the dislocation creep rate, constrained GB creep would be active and adjust this situation, see Sect. 5.4.

From now on in this section, it will be assumed that the creep data in Fig. 5.1 are controlled by dislocation creep. Since primary creep data are available at 700 °C, the analysis will be concentrated to that temperature. First a model is needed for stationary creep. Strain induced vacancies are taken into account according to Eq. (2.37)

$$\frac{\Delta c}{c_0} = 0.5\frac{\sqrt{2}K_{sub}^2\dot{\varepsilon}b^2}{D_{self}}\frac{G}{\sigma} \tag{5.38}$$

K_{sub} provides a relation between the subgrain size and the stress, Eq. (8.4). The strain rate in Eq. (5.31) is used in Eq. (5.38). Austenitic stainless have typically a low stacking fault energy which is important to take into account with the help of Eq. (3.30). These assumptions are the same as in a model for pure Ni, Sect. 2.8 [38], which is expected to have similar properties. The effect of dislocation dipoles have been taken into account. It increases the climb mobility by a factor f_{dip}

$$f_{\text{dip}} = 1 + 2\rho d_{\text{dip}}^2 \tag{5.39}$$

where d_{dip} is the distance between the dislocations in a dipole which is set to 1×10^{-7} m. In Sect. 2.8, pipe-diffusion is taken into account instead, which gives an almost identical effect. This effect is of special importance at high stresses. This expression can be derived in the same way as Eq. (2.13). The constant term in Eq. (5.39) raises the stress exponent at higher stresses by 2. The solid solution hardening due to Mo is taken into account by adding 50 kJ/mol to the activation energy following the discussion above. In the model for the non-stationary behavior, Eq. (5.32), the value for $\sigma_y/K(T) = 0.02$ has been selected to satisfy the criterion (5.36). The Ω value in the exponent in Eq. (5.32) has been determined with the help of Eq. (5.35). Quite a high value of $\Omega = 800$ is obtained.

Predictions of the creep strain during primary creep with the help of Eq. (5.33) are given in Fig. 5.2.

As can be seen that a reasonable representation of the experimental data is obtained. The strain rate versus time is shown in Fig. 5.3a.

Fully straight lines are found in the double logarithmic diagram in Fig. 5.3a indicating that the phi-model is satisfied, see Sect. 3.2. The slope of the strain rate versus time curves is 0.8. The stress exponent is 1. The corresponding strain rate versus strain curves are presented in Fig. 5.3b. Approximately straight lines are obtained. However, the slope is considerably higher than for the time dependence varying from 2 to 4.5. The stress exponent is close to 7 so it is the same as for stationary creep.

Results for strain rates as a function of stress are given in Fig. 5.4.

The stationary model has a stress exponent of 7 at high stresses. At low stresses the non-stationary primary creep models gives a stress exponent of 1 in agreement

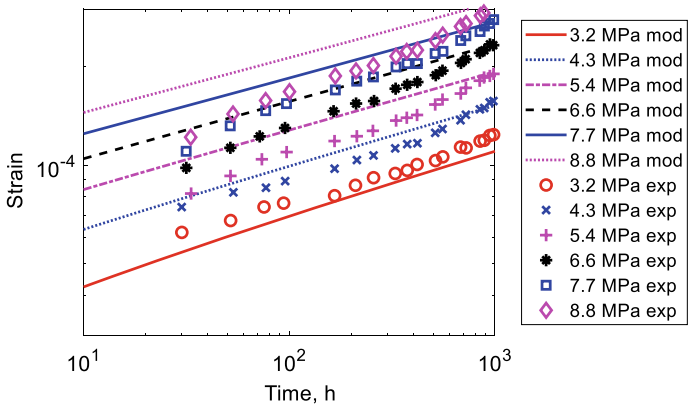

Fig. 5.2 Creep strain versus time at 700 °C for the austenitic stainless 17Cr12Ni2Mo steel 316H at low stresses during primary creep. Non-stationary model rates according to Eq. (5.33) compared to experimental data from [20]. Redrawn from [32] with permission of Elsevier

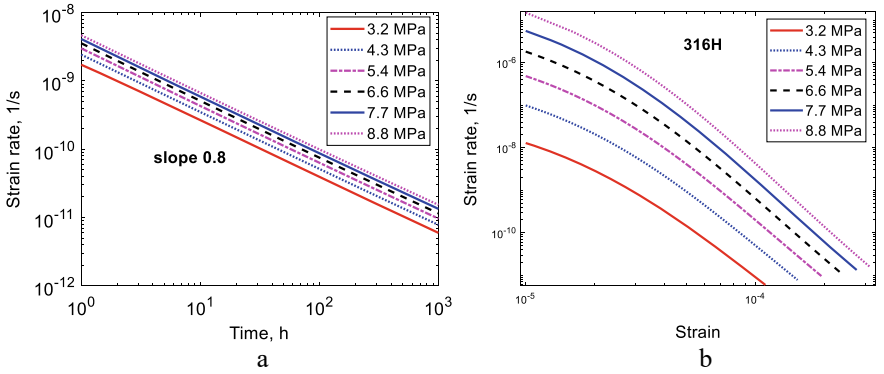

Fig. 5.3 Strain rate at 700 °C for the austenitic stainless 17Cr12Ni2Mo steel 316H at low stresses during primary creep. Non-stationary model rates according to Eq. (5.33); **a** strain rate versus time; **b** strain rate versus strain. **a** is redrawn from [32] with permission of Elsevier

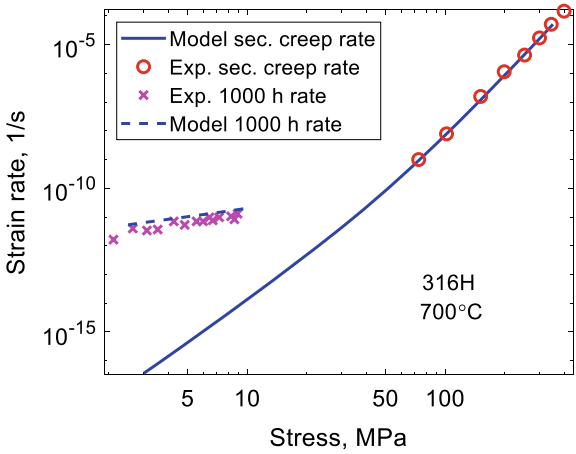

Fig. 5.4 Strain rate versus stress at 700 °C for the austenitic stainless 17Cr12Ni2Mo steel 316H with creep data from [20]. The full model line represents stationary creep rates and the dashed line non-stationary rates according to Eq. (5.33). Redrawn from [32] with permission of Elsevier

with observations. In Fig. 5.5 the time dependence of the strain rate versus stress curves is illustrated.

The strain rate decreases with increasing time in the primary stage. But even the longest time gives strain rates that are orders of magnitude above the stationary values, Fig. 5.4. At low stresses the activation energy in the model is 60 kJ/mol which is considerably less than the experimental value which is 140 kJ/mol. This value is almost the same as for grain boundary diffusion, which is 150 kJ/mol [34]. This is the expected value if Coble creep would have been the operating mechanism. The activation energy for stationary creep in the model is 340 kJ/mol, which is about 50 kJ/mol above the value for self-diffusion. The observed value is 420 kJ/mol. As discussed above that are good reasons to select a higher value than 50 kJ/mol for solid solution hardening, but due to lack of data this has not been done.

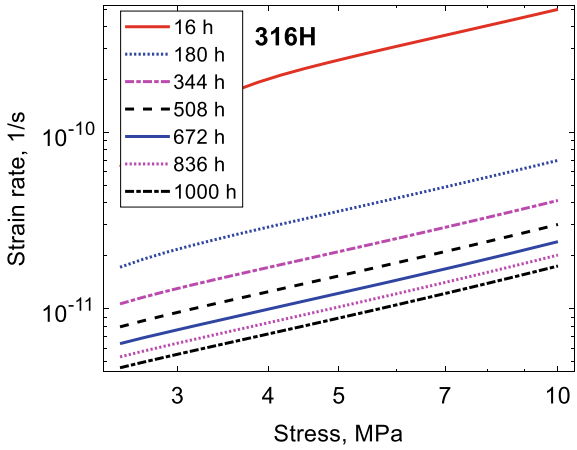

Fig. 5.5 Time dependence of the strain rate versus stress at 700 °C for the austenitic stainless 17Cr12Ni2Mo steel 316H at low stresses. Non-stationary model rates according to Eq. (5.33)

In summary, primary creep curves and their stress dependence of the creep rate can be described quite well with the model assuming dislocation creep. Thus, the model can explain the observations in a satisfactory way. It is clearly demonstrated that the stress exponent can be much lower during primary creep than during stationary creep. The activation energy is also lower during primary than during stationary creep although the model exaggerates the effect.

5.7 Creep in Aluminium at Very Low Stresses (Harper-Dorn Creep)

Creep at very low stresses and at very high temperatures in aluminum has received considerable interest in the scientific literature. The reason is that Harper and Dorn [14] looking for diffusional creep, in fact observed a stress exponent of 1 as expected but a creep rate that was about two orders of magnitude higher than the predicted one for diffusional creep. They drew the conclusion that they had observed dislocation creep with a stress exponent of 1. In two more recent papers available data have been summarized and analyzed [15, 19]. Kumar et al. [19] made also new tests for high purity aluminum to reduce the effect of non-stationary conditions. They could give a satisfactory explanation to most of the existing data. They found a creep exponent of 3 clearly indicating dislocation creep. The Harper and Dorn data also give this stress exponent when a threshold stress that they introduced was removed. Any indication of a threshold stress has not been found in more recent data.

In this section both stationary and non-stationary modeling will be presented taken from [32]. It has always been assumed that the controlling mechanism is dislocation creep. For stationary creep, the same model for aluminum as in Chap. 2 has been used, Eq. (5.31). The classical value for the self-diffusion coefficient with an activation energy of 142 kJ/mol has been applied. In the non-stationary model, Eq. (5.33), the

choice $\Omega = 40$ is taken directly from the formulae in Chap. 3. To satisfy the criterion (5.36) a value of $\sigma_y/K = 0.01$ has been chosen.

The results for the stress dependence of strain rate are given in Fig. 5.6.

The stationary creep model with a stress exponent of 3 can describe the bulk of creep of data. The only data that deviate significantly from the stationary curve are those of Barrett et al. [16]. They used testing times of 300–1000 h. In the other investigations longer testing times were utilized, which makes the results lying closer to the stationary values. It is evident that the modest deviations from the stationary curve can be well represented by the non-stationary model. How the results are approaching stationary conditions is illustrated in Fig. 5.7.

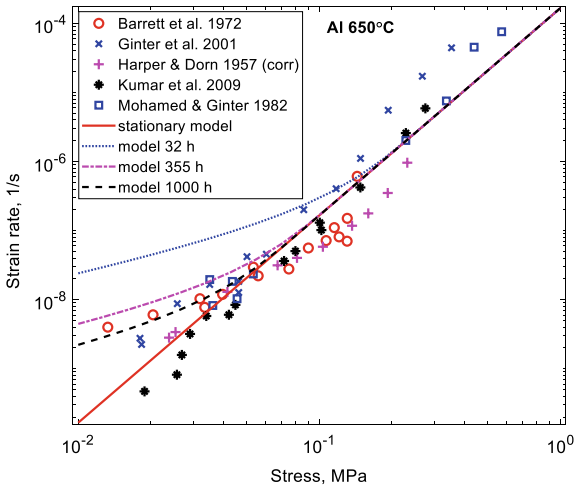

Fig. 5.6 Strain rate versus stress at 650 °C for pure aluminum. The full model line represents stationary creep rates and the dashed line non-stationary rates at three times according to Eq. (5.33). The five sources of the experimental data can be found in [19]. Redrawn from [32] with permission of Elsevier

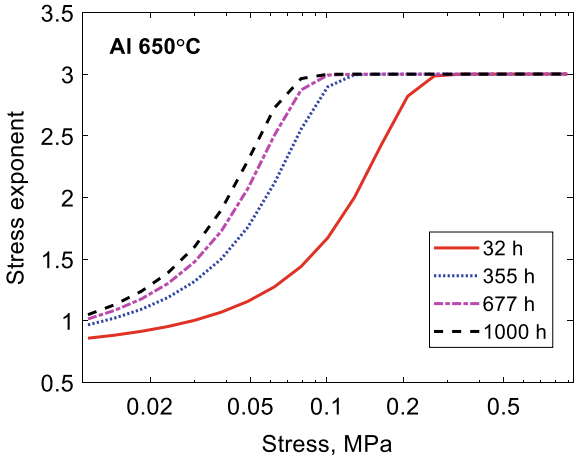

Fig. 5.7 Stress exponent versus stress at 650 °C for pure aluminum during non-stationary conditions at four times according to Eq. (5.33). Redrawn from [32] with permission of Elsevier

It can be seen from Fig. 5.7 that the values are close to stationary conditions. For stresses larger than 0.3, stationary creep has been reached even for the shortest time and the stress exponent is 3. Only for stresses below 0.03 MPa, stress exponents below 1.5 are found. The stress exponent clearly increases with increasing observation time.

Creep strain versus time curves are shown in Fig. 5.8.

The linear behaviour except at the highest stress is consistent with the phi-model. The variation of the strain rate with time and strain is demonstrated in Fig. 5.9.

The approximate straight lines again show that the phi-model is obeyed. The exception is the higher stresses where stationary conditions are reached at longer times or larger strains. This is the same behavior that is observed in Fig. 5.7.

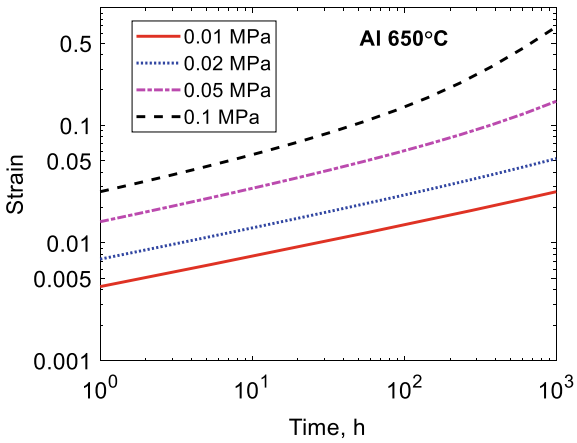

Fig. 5.8 Creep strain versus time at 650 °C for pure aluminum at different stresses according to Eq. (5.33)

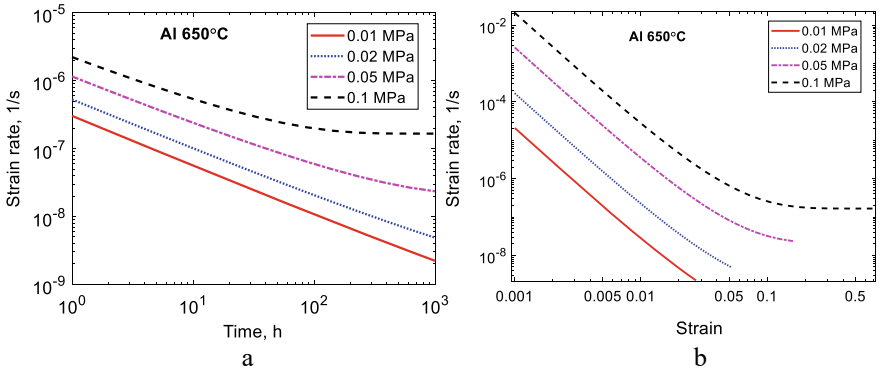

Fig. 5.9 Creep strain versus time **a** and versus strain **b** at 650 °C for pure aluminum at four stresses according to Eq. (5.33). **a** is redrawn from [32] with permission of Elsevier

These results above suggest that the high temperature creep of aluminum can be fully explained quantitatively based on ordinary dislocation creep. There is no need to refer to any special Harper-Dorn creep.

From Fig. 5.6 it can be seen that the basic creep model in Eq. (5.31) can describe the stationary creep rate quite accurately at least down to 0.02 MPa at 650 °C. The same model can represent creep data at 27 °C up to 50 MPa [39]. If the stress is raised from 0.02 to 50 MPa at 27 °C, the creep rate is increased by 21 orders of magnitude, see Table 5.1. The corresponding increase at 650 °C is 13 orders of magnitude. In the same way if the temperature is raised from 27 to 650 °C at 0.02 MPa, the creep rate is enhanced 17 orders of magnitude. At 50 MPa the increase is 9 orders of magnitude. Thus, Eq. (5.31) can cope with very large variation in the strain rate over a range of conditions. This is clearly strong justification for the validity of the creep model.

More recently, annealing experiments have been performed for aluminum single crystals by Smith et al. [40]. Even after long annealing times the dislocation density never fell below 1×10^9 1/m^2. With the help of the Orowan equation for the deformation, they suggest that this would give a stress exponent of 1, recovering Harper-Dorn creep. A constant dislocation density would imply that recovery of dislocations would be blocked. But if recovery is blocked, creep is not possible. Without recovery there would be a continuous increase in the dislocation density until the deformation stops as observed for many alloys at ambient temperatures. In addition, several other studies (some of which are summarized in [40]) have observed that the dislocation density varies with stress and that the dislocation density can be much below 1×10^9 1/m^2, see for example [19]. Furthermore, creep of aluminum can quantitatively be described from ambient temperatures, Sect. 2.7 to close to the melting temperature, see above, with the help of the creep-recovery theory. The observations in [40] cannot be explained at present.

Table 5.1 Creep rate ratios of aluminum

Temperature, °C	Stress, MPa	Creep rate ratio, stress	Creep rate ratio, temperature
27	0.02 → 50	2×10^{21}	
650	0.02 → 50	6×10^{13}	
27–>650	0.02		1×10^{17}
27–>650	50		4×10^9

5.8 Creep in Copper at Low Stresses

5.8.1 Creep of Cu-OFP at 600 °C

Creep tests of copper at very low stresses at 600 °C were performed at the author's laboratory many years ago but the results have only been published recently [41]. The material used was oxygen free copper alloyed with 54 wt. ppm P, Cu-OFP. The material had good purity. All other elements than Cu and P had a total amount of 30 wt. ppm. The batch had the designation 500. The detailed composition of the batch can be found in [42]. The grain size of the material was 100 μm. Three tests were carried out at 1, 1.5 and 2 MPa. The testing times were between 12000 and 17000 h. The conditions were selected to be well inside the stress range for diffusional creep. Results for the stress dependence of the strain rate are shown in Fig. 5.10.

The experimental data give a stress exponent of 3. A comparison to the model for stationary creep for Cu-OFP, Eq. (5.31) is given. It is evident that the model gives strain rate values that are quite close but with a slightly higher stress exponent of 4. For pure Cu without P the creep rate according to the stationary model is almost an order of magnitude higher and the stress exponent is 3.

In the primary creep model, Eq. (5.33), Ω has been selected according Eq. (5.35). For σ_y and K the room temperature values in [42] have been used. These values for σ_y and K satisfy the criterion (5.36). In Fig. 5.11, the strain rate versus time is illustrated for the test at 1.5 MPa.

Distinct primary creep is observed. Both the experiments and the predictions follow the phi-model. Thus, there are three ways that demonstrate that dislocation creep is involved; (i) a stress exponent of 3; (ii) the results are in agreement with the predictions for stationary dislocation creep; (iii) well-developed primary creep is present.

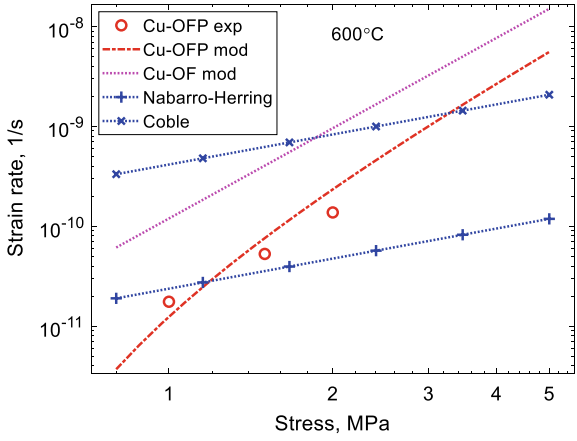

Fig. 5.10 Creep rate versus stress at 600 °C for Cu-OFP. Model values for stationary creep for Cu-OFP and for pure Cu without P (Cu-OF). Model results for diffusional creep are also included

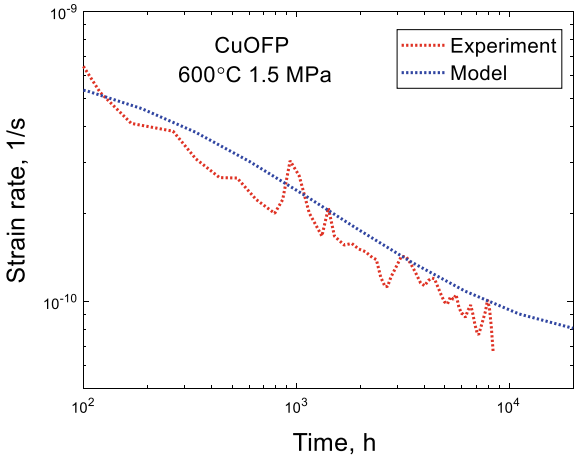

Fig. 5.11 Creep rate versus time at 600 °C and 1.5 MPa for Cu-OFP. Model values according to (5.33)

The basic stationary creep can describe creep rate values down to 1 MPa at 600 °C, Fig. 5.10. The model can also represent creep data at 75 °C up to 180 MPa, Fig. 6.6. This involves a large variation in the creep rate. Raising the stress from 1 to 180 MPa increases the creep rate by 21 orders of magnitude according to Eq. (5.31), Table 5.2. The corresponding increase at 600 °C is 13 orders of magnitude. There is also an increase due to change in temperature, which is 15 order of magnitude at 1 MPa and 9 orders of magnitude at 180 MPa.

These wide ranges of creep rate are of the same order as those for aluminum, Table 5.1. Which of the ratios in Tables 5.1 or 5.2 that is chosen is not important. The high ratios demonstrate that the basic creep model can cope with a wide range of conditions. Since the model was originally developed for creep close to ambient temperature at high stresses [31], the applicability at high temperatures and low stresses can be seen as a possibility to extrapolate over many order of magnitude in creep rate. It is clearly a strong justification for the validity of the basic creep model.

In Fig. 5.10, the classical models for diffusional creep are compared with the observations. It is evident that the model for Coble creep significantly overestimates the creep rate and that applies to Nabarro-Herring creep as well but to a less extent. Consequently, there must be one or more mechanisms that strongly block the diffusional processes. Such a diffusion mechanism is not easy to identify. P is known to raise the diffusion coefficients in both the bulk and in the grain boundaries [43], so

Table 5.2 Creep rate ratios of copper

Temperature, °C	Stress, MPa	Creep rate ratio, stress	Creep rate ratio, temperature
75	$1 \rightarrow 180$	4×10^{21}	
600	$1 \rightarrow 180$	2×10^{13}	
$75 \rightarrow 600$	1		6×10^{15}
$75 \rightarrow 600$	180		2×10^{9}

that effect works in the wrong way. Zhevnenko shows that surface active elements like P reduces the diffusional creep rate, but fairly large amounts of alloying elements are needed to give a significant effect [44]. Solid solution hardening due to P gives a back stress of 0.4 MPa at 600 °C [45]. This is the main reason why the stationary curve for Cu-OFP in Fig. 5.10 is lower than that for pure Cu. If dislocations control the amount of vacancies that escapes the grain boundaries, the solid solution hardening would be expected to be the same in the bulk and the grain boundaries. This effect is represented by the difference in the stationary creep rate between Cu with and without P. Thus, this would explain a part of the blocking of diffusional creep. P is fully in solid solution so there is no effect of particles. It has been suggested that if the curvature of the dislocation is too small, the grain boundary dislocations become immobile. This gives a back stress of [25, 46]

$$\sigma_{\text{curv}} = \frac{\tau_{\text{L}}}{bd_{\text{grain}}} \tag{5.40}$$

where τ_{L} is the dislocation line tension. For the case in Fig. 5.10, σ_{curv} is equal to 0.05 MPa, which is negligible. The remaining discrepancy for Coble creep is possibly due to constrained grain boundary creep, Sect. 5.4.

5.8.2 *Creep of Copper at 820 °C*

In one of the first attempts to measure diffusional creep, Burton and Greenwood studied pure copper at 820 °C [22]. Some of their results for a grain size of 35 μm are shown in Fig. 5.12.

Below 5 MPa their data gave a stress exponent close to 1. Above 5 MPa, the stress exponent is 5. The values for the classical Coble and Nabarro-Herring models

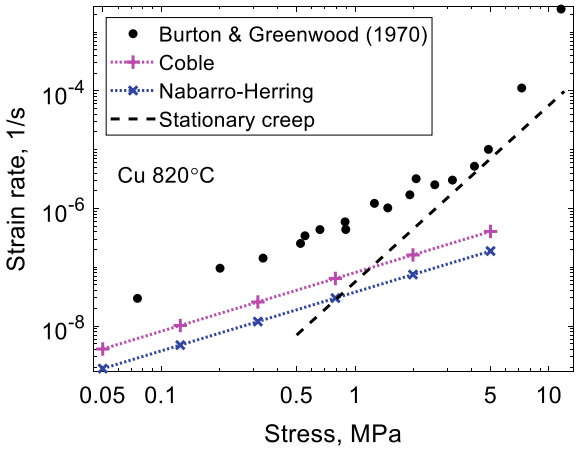

Fig. 5.12 Creep rate versus stress at 820 °C for Cu. Experimental data from [22]. Coble and Nabarro-Herring creep according to Eq. (5.10), stationary creep model according to (5.31). Redrawn from [41] with permission of Elsevier

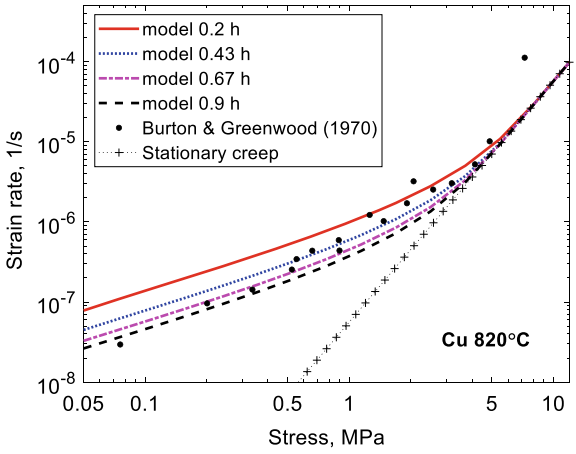

Fig. 5.13 Creep rate versus stress at 820 °C for Cu. Experimental data from [22]. Stationary and non-stationary creep models according to (5.31) and (5.33). Redrawn from [41] with permission of Elsevier

are quite close to the experimental data at low stresses. Burton and Greenwood suggested that the low stress behavior was controlled by Nabarro-Herring creep but with the diffusion coefficients that are available today, the Coble creep values are even closer. With a stress exponent of 5 at stresses above 5 MPa, dislocation creep must be controlling. It is interesting to note that the stationary creep model in Eq. (5.31) matches the position of the change in stress exponent quite well, but the stress exponent in the stationary model is 3.

It will now be analyzed whether non-stationary conditions could have been of importance in this study [41]. Detailed analysis shows that transition to the semi-stationary stage occurs later than given by Eq. (5.35) so the Ω value has been reduced by a factor of 2 to satisfy these findings in the non-stationary model (5.33). For σ_y/K a value of 0.01 has been chosen to ensure that the criterion (5.36) is fulfilled. In [22] very short testing times were used of about 0.4 h. The results for stress dependence of the creep rate are given in Fig. 5.13.

Results for testing times between 0.2 and 0.9 h are shown. The non-stationary values fall in the same range as the experimental data. The variation of the stress exponent is presented in Fig. 5.14.

Below 1 MPa, the stress exponent is close to unity. From 1 to 5 MPa the stress exponent increases to the stationary value of 3. The strain variation with time is reproduced in Fig. 5.15a.

The creep curves are consistent with the observation in [22], see [41]. For example, a strain of 0.002 is reached after 0.5 h for a stress of 1 MPa. In Fig. 5.15b the time dependence of the strain rate is given. It is evident that stationary conditions are reached at the two highest stresses at "longer" times.

It is clear that the data in Fig. 5.12 can be explained either with diffusional creep or with non-stationary dislocation creep. One argument against diffusional creep is the short testing times that would give non-stationary effects. Another argument is that the purity of the investigated alloy is modest with a total impurity content of 167 wt. ppm. This should be compared with the copper in Sect. 5.8.1, where

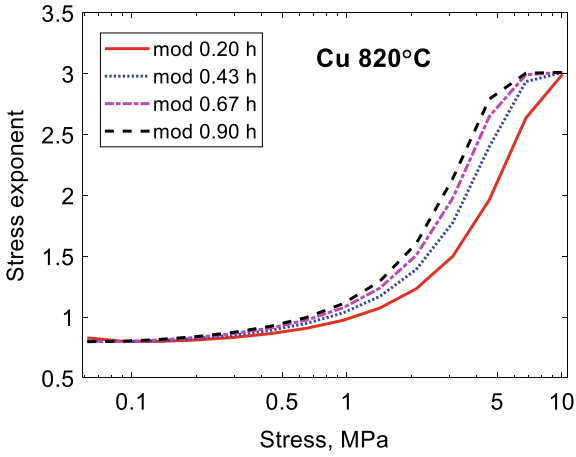

Fig. 5.14 Stress exponent versus stress at 820 °C in Cu at four testing times. Non-stationary creep models according to Eq. (5.33). Redrawn from [41] with permission of Elsevier

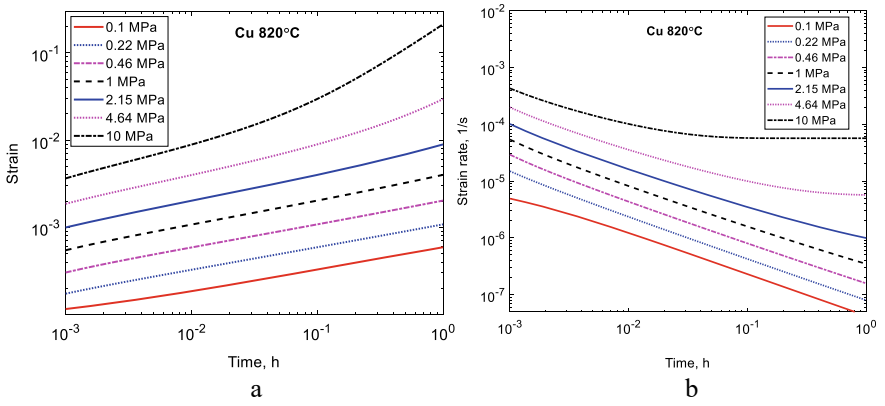

Fig. 5.15 Strain **a** and strain rate **b** versus time at 820 °C in Cu at seven stresses. Non-stationary creep model according to (5.33)

the impurity content was 30 wt. ppm and the P content 54 wt. ppm. Why would diffusional creep be blocked by element additions in the latter but not in the former case? The paper [22] has been criticized in the literature, for example, for being performed in a temperature range where the microstructure is not stable [4, 12]. This might not be important due to the short testing times. However, there are arguments in [22] in favor of diffusional creep. For example, the correct grain size dependence if Nabarro-Herring creep is controlling (which however is not the case if Coble creep is controlling). It is not possible to decide which creep mechanisms that is the correct one and it is not the aim of this book to try to make that decision. Instead, the main message is that dislocation creep often occurs in parallel and in competition with diffusional creep.

5.8.3 Creep of Copper at 480 °C

McKnee et al. have made creep tests of copper at low stresses [9]. Most tests were performed at 480 ºC probably for the same material used by Burton and Greenwood but with a grain size of 55 μm. These results are compared with the non-stationary model, Eq. (5.33). The parameter values are taken directly from the basic model ($\sigma_y = 0.01$ MPa, $K(T) = 69$ MPa, $\Omega = 32$). The results in [9] are compared to the model in Fig. 5.16.

Below 3 MPa the results by McKnee et al. give a stress exponent of 1 and above 3 MPa a stress exponent of 2. They attribute this change of stress exponent to a transition from diffusional creep to dislocation creep. A comparison to stationary creep is provided in Fig. 5.17.

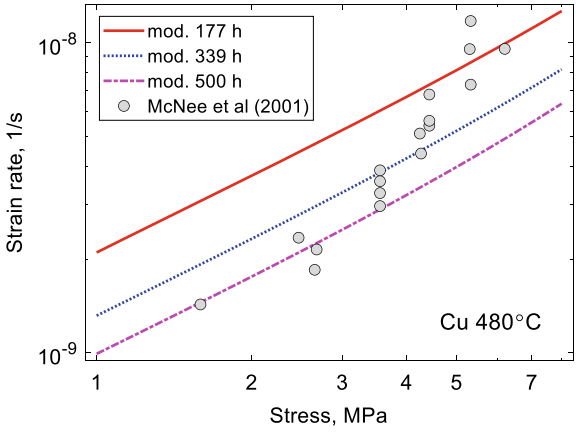

Fig. 5.16 Creep rate versus stress at 480 °C for Cu. Experimental data from [9]. Non-stationary creep model according to Eq. (5.33)

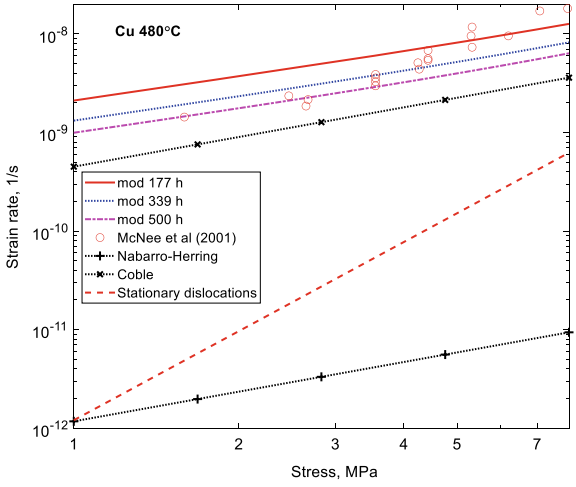

Fig. 5.17 Creep rate versus stress at 480 °C for Cu. Experimental data from [9]. Stationary and non-stationary creep models according to Eqs. (5.31) and (5.33). Classical diffusional creep models are given, Eq. (5.10)

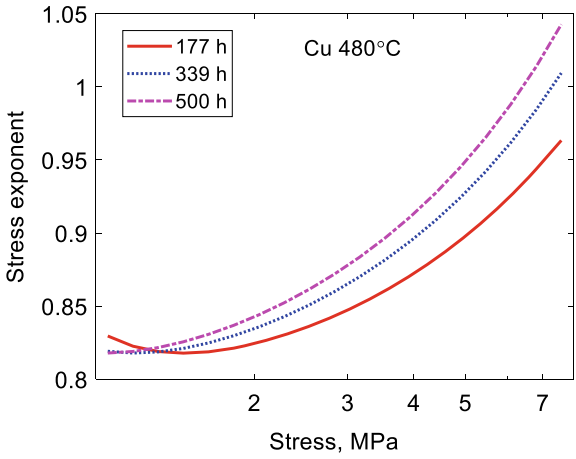

Fig. 5.18 Stress exponent for the creep rate versus stress at 480 °C for Cu for three testing times. Non-stationary creep model according to Eq. (5.33)

Results for stationary creep according to Eq. (5.31) are 1.5 orders of magnitude or more below the results in [9]. Considering the precision of the prediction of stationary creep in Fig. 5.10, the results in [9] must represent non-stationary creep. The non-stationary model, Eq. (5.33), generates values that are in agreement with the observations in [9] considering the length of testing times that were used in that investigation. The stress exponent in the non-stationary model is illustrated in Fig. 5.18.

The stress exponent in the range of data of [9] is about 1. There is a slight increase with stress but it is not enough to explain the observed increase to 2. The stationary creep values are simply too far below the observation to give such an increase. The Coble results in Fig. 5.17 are close to both the values in [9] and the non-stationary results. The activation energy predicted from the non-stationary model, Eq. (5.33) is shown in Fig. 5.19.

In the model, lattice diffusion with an activation energy of 198 kJ/mol from [47] is used. In spite of this, the non-stationary model gives a value of about 70 kJ/mol at 480 °C. Via step change tests, McKnee et al. found a creep activation energy of 99 ± 5 kJ/mol. Both these values are close to the accepted value for grain boundary diffusion of 84.5 kJ/mol [48] which is the relevant value for Coble creep. It can be seen that the mechanical data in [9] can be explained at least partially with the help of non-stationary dislocation creep.

5.9 Summary

- One issue when performing creep tests at low stresses is to ensure that stationary conditions have been reached. At normal stresses when tests run to failure the minimum creep rate usually gives a good estimate of the stationary rate. However, creep tests at low stresses when the stress exponent is close to unity practically

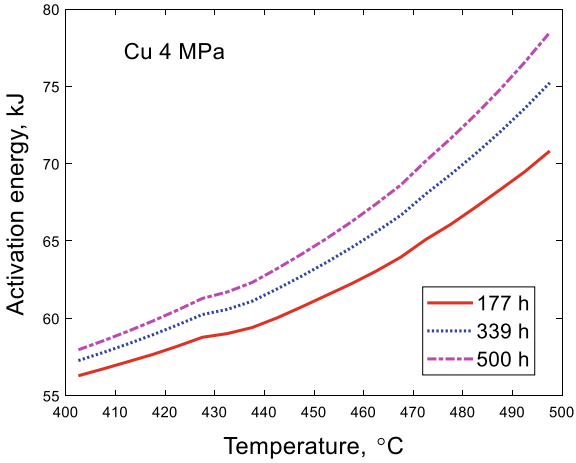

Fig. 5.19 Activation energy for the creep rate versus temperature for Cu at three testing times. Non-stationary creep model according to Eq. (5.33)

never are taken to failure. Often this is simply not possible because the estimated rupture time could be 10 years or more.

- Stationary creep rates have traditionally been the basis of identifying operating mechanisms, for example for distinguishing between diffusional creep, power-law dislocation creep and power-law break-down. For a long time only empirical dislocation creep models were available but this identification could still be made as long as stationary conditions could be ascertained. However, at low stresses it must in general be assumed that a stationary state has not been reached during the testing. It is then essential to use non-stationary models.
- In recent years basic dislocation creep models that can cope also with the primary stage have been formulated. These models are at least partially predictable and that is essential to analyze the data. During the primary stage the creep rate drops quickly. Where in the primary stage the test is stopped must be determined.
- Traditionally it has been assumed that a stress exponent close to 1 should imply that diffusional creep is active. The classical models for diffusional creep are simple and well established. They give well-defined stress, temperature and grain size dependence. In spite of this it has been difficult to obtain agreement with the models in many cases. In several classical studies for pure metals, the diffusional models overestimate the creep rate by two orders of magnitude. Since quite accurate diffusion coefficients are available, the deviations cannot be accounted for by lack of precision. Two alternatives then remain. Either the observations are non-stationary dislocation creep or non-stationary diffusional creep.
- Experimental results for an austenitic stainless at 700 °C gave a stress exponent of 1, but the presence of primary creep and a stress exponent of 4.5 in related stress change tests clearly demonstrated that dislocation creep was the operating mechanism. The same results were found for Cu at 600 °C since the observed stress exponent was 3 and distinct primary creep was observed. In spite of these quite clear verifications that dislocation creep was the controlling mechanism,

the classical Coble creep model predicted creep rates one order of magnitude higher than the observed ones. Consequently, Coble creep must be blocked by one or more mechanisms. If Coble creep is controlled solely by diffusion in the grain boundaries, this is virtually impossible to account for. Several authors have proposed that the motion of vacancies is controlled by grain boundary dislocations. If this assumption is correct, and the amount of solid solution hardening is the same for GB and bulk dislocations, the observations are at least partially possible to explain although very large blocking effects would be required since the mobility of the grain boundary dislocations is very high. The more likely explanation is due to constrained grain boundary creep. see next bullet [41].

- Any creep mechanism that is located in the grain boundaries is proposed to be accompanied by bulk deformation. Such mechanisms are superplasticity due to grain boundary sliding, grain boundary dislocation creep and Coble creep. Thus, the bulk creep rate must be at least of the same magnitude as the creep in the grain boundaries to accommodate local strain changes. This is referred to as *constrained grain boundary creep*. This has important implications. The Coble creep rate can never exceed the bulk creep rate by a significant margin. In addition, since the Coble creep rate must be adapted to the bulk rate, it will show primary creep.
- A primary creep model has been used to describe dislocation creep with low creep exponents. The model has been applied successfully to an austenitic stainless steel, to pure Al and to pure Cu. It is shown that dislocation creep can be active in stress and temperature ranges that traditionally have been attributed only to diffusional creep. The low stress exponents observed is a result of stationary conditions not being reached. It is demonstrated that if non-stationary conditions are assessed the apparent activation energy can be much lower than the lattice diffusion activation energy used in the model.
- Creep at very high temperature and low stresses for pure Al has in the past been considered as a special case with the designation Harper-Dorn after the researchers that first proposed it. For the first time a basic model has been used to describe data from a number of investigations for this type of creep. The model successfully shows that the bulk of data can be represented by a stationary model giving a stress exponent of 3 in agreement with observations. The data that deviate from this behavior can be handled with the non-stationary model. In agreement with results in the literature, there is no longer any need to consider this phenomenon as something special, since the dislocation creep model can describe these results in a similar way as for other alloys.
- It has been demonstrated that the basic models for primary and secondary creep can accurately describe experimental data at high temperatures and low stresses. For secondary creep the model parameters are identical to the ones used at lower temperature. Thus, for aluminum the application of the basic creep model has been verified from 50 MPa at room temperature to 0.02 MPa at 650 °C. For copper the corresponding range is from 180 MPa at 75 °C to at least 1 MPa at 600 °C. For both the stress and temperature ranges, they represent a variation of in the creep rate over many orders of magnitude. For copper primary creep is accurately represented in the same range also without any change of parameter

values. These facts clearly show that the basic creep model can handle a wide range of experimental conditions. Primary creep of aluminum has not been investigated at ambient temperatures.

References

1. C. Herring, Diffusional viscosity of a polycrystalline solid. J. Appl. Phys. **21**, 437–445 (1950)
2. R.L. Coble, A model for boundary diffusion controlled creep in polycrystalline materials. J. Appl. Phys. **34**, 1679–1682 (1963)
3. M.E. Kassner, *Fundamentals of Creep in Metals and Alloys* (Butterworth-Heinemann, 2015)
4. O.A. Ruano, J. Wadsworth, J. Wolfenstine, O.D. Sherby, Evidence for Nabarro-Herring creep in metals: fiction or reality? Mater. Sci. Eng. A **165**, 133–141 (1993)
5. T. Sritharan, H. Jones, The creep of Beta-Cobalt at low stresses. Acta Metall. **27**, 1293–1300 (1979)
6. D.J. Towle, H. Jones, The creep of alpha-iron at low stresses. Acta Metall. **24**, 399–407 (1976)
7. T.G. Langdon, A method of distinguishing between diffusion creep and Harper-Dorn creep at low stress levels. Scripta Mater. **35**, 733–737 (1996)
8. R.L. Squires, R.T. Weiner, M. Phillips, Grain-boundary denuded zones in a magnesium-12 wt % zirconium alloy. J. Nucl. Mater. **8**, 77–80 (1963)
9. K.R. McNee, G.W. Greenwood, H. Jones, Microstructural evidence for diffusional creep in copper using atomic force microscopy. Scripta Mater. **44**, 351–357 (2001)
10. K.R. McNee, G.W. Greenwood, H. Jones, Observation and interpretation of some microstructural features of low stress creep. Scripta Mater. **47**, 619–623 (2002)
11. K.R. McNee, G.W. Greenwood, H. Jones, The effect of stress orientation on the formation of precipitate free zones during low stress creep. Scripta Mater. **46**, 437–439 (2002)
12. O.A. Ruano, O.D. Sherby, J. Wadsworth, J. Wolfenstine, Rebuttal to "In defense of diffusional creep." Mater. Sci. Eng. A **211**, 66–71 (1996)
13. J. Wadsworth, O.A. Ruano, O.D. Sherby, Denuded zones, diffusional creep, and grain boundary sliding. Metall. Mater. Trans. A **33**, 219–229 (2002)
14. J. Harper, J.E. Dorn, Viscous creep of aluminum near its melting temperature. Acta Metall. **5**, 654–665 (1957)
15. M.E. Kassner, P. Kumar, W. Blum, Harper-Dorn creep. Int. J. Plast **23**, 980–1000 (2007)
16. C.R. Barrett, E.C. Muehleisen, W.D. Nix, High temperature-low stress creep of Al and Al+0.5%Fe. Mater. Sci. Eng. **10**, 33–42 (1972)
17. F.A. Mohamed, T.J. Ginter, On the nature and origin of Harper-Dorn creep. Acta Metall. **30**, 1869–1881 (1982)
18. W. Blum, P. Eisenlohr, F. Breutinger, Understanding creep—A review. Metall. Mater. Trans. A **33**, 291–303 (2002)
19. P. Kumar, M.E. Kassner, W. Blum, P. Eisenlohr, T.G. Langdon, New observations on high-temperature creep at very low stresses. Mater. Sci. Eng. A **510–511**, 20–24 (2009)
20. L. Kloc, V. Sklenička, J. Ventruba, Comparison of low stress creep properties of ferritic and austenitic creep resistant steels. Mater. Sci. Eng. A **319–321**, 774–778 (2001)
21. L. Kloc, V. Sklenička, Confirmation of low stress creep regime in 9% chromium steel by stress change creep experiments. Mater. Sci. Eng. A **387–389**, 633–638 (2004)
22. B. Burton, G.W. Greenwood, The contribution of grain-boundary diffusion to creep at low stresses. Metal Sci. J. **4**, 215–218 (1970)
23. M.F. Ashby, R.A. Verrall, Diffusion-accommodated flow and superplasticity. Acta Metall. **21**, 149–163 (1973)
24. G.W. Greenwood, A formulation for anisotropy in diffusional creep, Proc. Roy. Soc. A **A436**, 187–196 (1992)

25. E. Arzt, M.F. Ashby, R.A. Verrall, Interface controlled diffusional creep. Acta Metall. **31**, 1977–1989 (1983)
26. M.F. Ashby, On interface-reaction control of Nabarro-Herring creep and sintering. Scr. Metall. **3**, 837–842 (1969)
27. D. Francke, W. Pantleon, P. Klimanek, Modelling the occurrence of disorientations in dislocation structures. Comp. Mater. Sci. **5**, 111–125 (1996)
28. P. Ambrosi, C. Schwink, Slip line length of copper single crystals oriented along [100] and [111]. Scr. Metall. **12**, 303–308 (1978)
29. L.C. Lim, On the elastic properties of grain boundary dislocations. Acta Metall. **35**, 163–169 (1987)
30. A.H. Chokshi, Unusual stress and grain size dependence for creep in nanocrystalline materials. Scripta Mater. **61**, 96–99 (2009)
31. R. Sandstrom, Basic model for primary and secondary creep in copper. Acta Mater. **60**, 314–322 (2012)
32. R. Sandström, Creep at low stresses in aluminium (Harper-Dorn) and in an austenitic stainless steel with a stress exponent of 1. Mater. Today Commun. **36**, 106556 (2023)
33. A.F. Smith, G.B. Gibbs, The volume and grain-boundary diffusion of iron in 20 Cr/25 Ni/Nb stainless steel. Metal Sci. J. **2**, 47–50 (1968)
34. M. Mizouchi, Y. Yamazaki, Y. Iijima, K. Arioka, Low temperature grain boundary diffusion of chromium in SUS316 and 316L stainless steels. Mater. Trans. **45**, 2945–2950 (2004)
35. F. Delannay, Contribution of the nucleation and recovery of disconnections to shear viscosity in diffusional creep. Materialia **20** (2021)
36. P.A. Korzhavyi, R. Sandström, First-principles evaluation of the effect of alloying elements on the lattice parameter of a 23Cr25NiWCuCo austenitic stainless steel to model solid solution hardening contribution to the creep strength. Mater. Sci. Eng. A **626**, 213–219 (2015)
37. Data Sheet on the Elevated-Temperature Properties of 18Cr–8Ni–Mo Stainless Steel Tubes for Boiler and Heat Exchangers (SUS 316H TB), National Research Institute for Metals Tokyo, Japan, Report No. 6B (2000)
38. R. Sandström, J. Zhang, Modeling the creep of nickel. J. Eng. Mater. Technol. **143**(4), 041011–1 (2021)
39. S. Spigarelli, R. Sandström, Basic creep modelling of aluminium. Mater. Sci. Eng. A **711**, 343–349 (2018)
40. K.K. Smith, M.E. Kassner, P. Kumar, Long-term annealing of high purity aluminum single crystals: new insights into Harper-Dorn creep. Mater. Sci. Eng. A **705**, 1–5 (2017)
41. R. Sandström, Primary creep at low stresses in copper. Mater. Sci. Eng.: A **873**, 144950 (2023)
42. R. Sandstrom, Extrapolation of creep strain data for pure copper. J. Test. Eval. **27**, 31–35 (1999)
43. R. Sandström, R. Wu, J. Hagström, Grain boundary sliding in copper and its relation to cavity formation during creep. Mater. Sci. Eng. A **651**, 259–268 (2016)
44. S.N. Zhevnenko, Effect of surface-active metallic impurities on diffusion creep of polycrystalline copper. Mater. Lett. **282** (2021)
45. R. Sandstrom, H.C.M. Andersson, The effect of phosphorus on creep in copper. J. Nucl. Mater. **372**, 66–75 (2008)
46. B. Burton, Grain boundary dislocation geometry during diffusional creep. Mater. Sci. Technol. (United Kingdom) **2**, 1202–1204 (1986)
47. G. Neumann, V. Tölle, C. Tuijn, Monovacancies and divacancies in copper Reanalysis of experimental data. Phys. B **271**, 21–27 (1999)
48. T. Surholt, C. Herzig, Grain boundary self-diffusion in Cu polycrystals of different purity. Acta Mater. **45**, 3817–3823 (1997)